

Neutrino Mass Inference from SZ Surveys

Meir Shimon¹, Sharon Sadeh², and Yoel Rephaeli^{1,2}

¹ *Center for Astrophysics and Space Sciences, University of California,
San Diego, 9500 Gilman Drive, La Jolla, CA, 92093-0424 and*

² *School of Physics and Astronomy, Tel Aviv University, Tel Aviv 69978, Israel*

The growth of structure in the universe begins at the time of radiation-matter equality, which corresponds to energy scales of $\sim 0.4\text{eV}$. All tracers of dark matter evolution are expected to be sensitive to neutrino masses on this and smaller scales. Here we explore the possibility of using cluster number counts and power spectrum obtained from ongoing SZ surveys to constrain neutrino masses. Specifically, we forecast the capability of ongoing measurements with the PLANCK satellite and the ground-based SPT experiment, as well as measurements with the proposed EPIC satellite, to set interesting bounds on neutrino masses from their respective SZ surveys. We also consider an ACT-like CMB experiment that covers only a few hundred deg^2 also to explore the tradeoff between the survey area and sensitivity and what effect this may have on inferred neutrino masses. We find that for such an experiment a shallow survey is preferable over a deep and low-noise scanning scheme. The precision with which the total neutrino mass can be determined from SZ number counts and power spectrum is limited mostly by uncertainties in the basic cosmological parameters, the mass function of clusters, and their mean gas mass fraction; all these are explicitly accounted for in our statistical Fisher-matrix treatment. We find that projected results from the PLANCK SZ survey can, in principle, be used to determine the total neutrino mass with a (1σ) uncertainty of 0.28eV , if the detection limit of a cluster is set at the 5σ significance level. This is twice as large as the limits expected from PLANCK CMB lensing measurements. The corresponding limits from the SPT and EPIC surveys are $\sim 0.44\text{eV}$ and $\sim 0.12\text{eV}$, respectively. Mapping an area of 200 deg^2 , ACT measurements are predicted to attain a 1σ uncertainty of 0.61 eV ; expanding the observed area to $4,000\text{ deg}^2$ will decrease the uncertainty to 0.36 eV .

PACS numbers:

I. INTRODUCTION

The temperature anisotropy and polarization state of the CMB constitute a unique window on the physical state of the universe in the era of recombination ($z \approx 1100$), $\sim 400,000$ years after the big bang. Measurements with the COBE and WMAP satellites, along with a host ground-based and balloon-borne experiments, have led to impressively precise values of the basic cosmological parameters. Other cosmological probes, sensitive to certain combinations of these parameters, supplement CMB data, significantly reduce parameter degeneracies, and provide some control of systematic uncertainties. A major advantage of the CMB is its well understood underlying physics, a fact that justifies its distinction as the most precise cosmological probe. This said, it is also well recognized that the diagnostic power of the primary CMB anisotropy, whose main features reflect conditions at recombination, is rather limited in constraining certain cosmological parameters. Measurements with the recently launched PLANCK satellite are cosmic-variance-limited up to $\ell \approx 2500$, and are therefore expected to reduce this limitation significantly by mapping the primary CMB anisotropy down to scales of a few arcminutes.

Neutrino masses are a good example for the need to sensitively map the primary CMB anisotropy at high ℓ . Below their Jeans scale, massive neutrinos free-stream and act as a hot dark matter (HDM) component, reducing the growth of the large scale structure (LSS) as compared with the evolution of structure in a pure cold dark matter (CDM) model. This characteristic neutrino signature provides a diagnostic measure that can be exploited to either determine or constrain their masses. Current cosmological constraints on neutrino masses come from the CMB temperature anisotropy e.g. [1,2], weak gravitational lensing [3-6], as well as galaxy [7-11] and $\text{Ly}\alpha$ surveys [12-15]. WMAP7 data already set an upper limit (at the 95% confidence level) of 0.58 eV on total neutrino mass [2]. This limit, which comes mainly from CMB constraints on the *early* integrated Sachs Wolfe (ISW) effect ($l < 200$), is related to the fact that the neutrino temperature at radiation-matter equality is $\approx 0.4\text{ eV}$ (in equivalent energy units), and that there are three active neutrino species. The ISW effect is associated with the kinematics of neutrinos at the time period between radiation-matter equality and recombination. This is an indirect probe of neutrino kinematics at, and prior to, last scattering. To improve on this bound, probes of neutrino kinematics at lower redshifts are required, where neutrino temperatures are lower (it can certainly be the case that a massive neutrino which is nonrelativistic today, was actually relativistic, i.e. freely streamed, at much higher redshifts). This may be achieved, for example, by employing lensing extraction of the CMB, e.g. [16-18].

The relatively strong bounds deduced from CMB data on the *total* neutrino mass should be contrasted with the

mass that would have provided closure density (of a hypothetical neutrino-dominated) universe, ≈ 45 eV, and to the actually measured value of the matter density parameter, $\Omega_{cdm} \approx 0.3$ (equivalently, ~ 5 eV per neutrino species if the entire dark matter was made up of neutrinos). From this perspective, the total neutrino mass is bounded to be lower than 4% (2σ) of all dark matter (DM). As a tracer of LSS, gravitational lensing of the CMB is a sensitive probe of any cosmological parameters that affect the formation or growth-rate of the perturbed background matter density.

Galaxy clusters are excellent probes of structure formation, and therefore can be used, in principle, for indirectly setting limits on neutrino masses through their dynamics and impact on structure formation. For this purpose, it has been suggested [19] that cluster number counts and cluster correlations can be used to set useful upper bounds on neutrino masses. These probes are sensitive to the evolution of structure down to the typical correlation scale of galaxy clusters, a few tens of Mpc, and are therefore sensitive to sub-eV neutrino masses. Lensing of the CMB with planned good sensitivity and high resolution experiments, e.g. [20,21] could do even better, perhaps even constrain the total neutrino mass, M_ν , at the 0.05 eV level. It is interesting to note that this level overlaps with the lower mass limit from neutrino oscillations, e.g. [22-24]. This implies that, to the level of confidence we have in these forecasts, in the not too distant future, neutrino masses and mass hierarchy will be resolved, if next generation CMB satellites (e.g. EPIC [20]) will indeed be launched. However, other probes are certainly of interest even if their respective precision levels cannot compete with the CMB lensing probe, since they can provide much needed consistency checks for systematics and parameter degeneracy breaking.

We have explored the possibility of determining neutrino masses from survey measurements of the SZ effect (Comptonization of the CMB by hot gas in clusters, e.g. [25-27]) by the currently operational ground-based SPT project, PLANCK satellite, and the proposed EPIC satellite mission. We also explored various scanning schemes for the ground-based ACT to gain some insight on how to optimize SZ surveys for neutrino mass inference. The basic motivation for doing so is provided by the fact that the SZ effect is a sensitive tracer of the evolution of the LSS. However, in contrast to the linear physics characterizing much of the evolution of the primary CMB anisotropy, the SZ effect is more model-dependent (e.g., mass-temperature scaling relation, gas mass fraction and spatial profile). A substantial source of uncertainty is the distribution of the entire cluster population in mass-redshift space, i.e. the mass function. This important function, whose specific shape and normalization reflect the details of the growth of density fluctuations, and the non-linear hierarchical collapse and mergers of sub-structures, can be best studied by state-of-the-art large-volume hydrodynamical cosmological simulations. Although very advanced, currently available computer codes predict a range of mass functions. At present, this mass function indeterminacy largely sets the precision limit of forecasting the total neutrino mass from cluster SZ number counts and power spectrum.

In this paper we discuss constraints on neutrino masses that can be obtained from SZ surveys alone. In particular, we determine how likely it will be for PLANCK, SPT and EPIC to constrain neutrino masses by using the sensitivity of cluster number counts and SZ power spectrum to neutrino masses. For the first time in this context, attention is given to the robustness of the results to the assumed fiducial neutrino mass. One of our main objectives is to check to what extent the upper limits on neutrino masses derived from SZ surveys are robust to modeling uncertainties and other systematics.

The paper is organized as follows. In section II we discuss the impact of massive neutrinos on the LSS with special emphasis on its manifestation in the transfer function and cluster mass function. Cluster number counts, correlation, and induced CMB anisotropy are described in section III. We lay out the methodology of our estimates for expected number counts and SZ power as a function of neutrino mass and address issues such as detection threshold, foregrounds, etc. along with a description of the Fisher matrix analysis used in this work in section IV. Our main results are presented in section V and further discussed in section VI.

II. NEUTRINO IMPACT ON GROWTH OF THE LSS

At a redshift 3200, the CMB and matter energy densities, together with the neutrino contribution, set the time of matter-radiation equality, t_{eq} . This transition preceded recombination, but not by much; thus, the universe was not purely matter-dominated at recombination. Consequently, gravitational potential wells could decay and induce the early ISW effect, which boosts the angular power spectrum of the CMB temperature anisotropy on multipoles that correspond to the horizon scale at recombination, i.e. $l \sim 100 - 200$. In other words, a_{rec}/a_{eq} , the ratio of the scale factors at recombination and matter-radiation equality is a measure of the linear growth of structure during the period between radiation-matter equality and recombination. This ratio clearly depends on neutrino masses. The fraction of total energy in the form of radiation (which would include neutrinos, if the total neutrino mass is below ~ 1 eV) at recombination determines the amplitude of the early ISW effect.

More stringent constraints on neutrino masses could, in principle, be obtained from the SZ effect. A massive neutrino that is nonrelativistic today [$m_\nu c^2 > kT_\nu(0)$], was relativistic at higher redshifts [$m_\nu c^2 < kT_\nu(z)$], and therefore could not easily cluster then, causing a relative suppression of structure formation compared to what would

be expected had this species been non-relativistic for the entire history of structure formation ($t > t_{eq}$). In principle, precise measurements of the LSS - for example, cluster number counts - can be used to place constraints on neutrino masses.

The evolution of structure in the matter-dominated era is described in terms of the matter power spectrum,

$$P_m(k, z) = Ak^n T^2(k, z), \quad (1)$$

with the primordial density fluctuation spectrum, Ak^n , where A is an overall normalization, n is the tilt of the power spectrum, and the transfer function, $T(k, z) = T(M_\nu; k, z)$. An important quantity gauging the amplitude of the processed power spectrum observed today is the mass variance parameter on a scale of $8Mpc\ h^{-1}$,

$$\sigma_8 = \int_0^\infty P_m(k, z) W^2(kR) k^2 \frac{dk}{2\pi^2}, \quad (2)$$

where $W(kR)$ is a window function, and $R = 8Mpc\ h^{-1}$. The latter quantity incorporates the physics of neutrino damping; thus, σ_8 is a function of not only A , n , but also of neutrino masses (via the transfer function), and indeed any other cosmological parameter which affects structure evolution on scales of few tens Mpc and lower. Because these scales are comparable to typical scales of diffusion damping of density fluctuations by neutrinos with small masses, we expect that M_ν and σ_8 will be anti-correlated. Since the SZ signature is a strong function of σ_8 , it is expected to be sensitive also to M_ν .

A. The Transfer Function

Quantitative description of the effects of neutrinos on the evolution of the LSS begins with a modification of the density fluctuation spectrum as described by the transfer function. Whereas the standard CDM transfer function is separable in the perturbation wave-number k and redshift z

$$T(k, z) = D(z) \tilde{T}(k) \quad (3)$$

where $D(z)$ is the linear growth factor and, e.g. [28],

$$\tilde{T}(k) = \frac{\ln(1 + 2.34q)}{2.34q} [1 + 3.89q + (16.1q)^2 + (5.46q)^3 + (6.71q)^4]^{-1/4} \quad (4)$$

and $q \equiv k/(\Omega_m h^2) Mpc^{-1}$, a mixed DM model generally cannot be cast in such a simple form. This is due to the redshift-dependence of the free-streaming scale, k_{FS} , which is determined by both neutrino mass and the redshift-dependent neutrino temperature, $T_\nu(z)$. A reasonable first approximation to the transfer function in the presence of neutrinos, is e.g., [29]

$$\begin{aligned} T^2(k, z) &\rightarrow D^2(z) \tilde{T}^2(k); & k < k_{nr} \\ T^2(k, z) &\rightarrow D(z)^{2-\frac{6}{5}f_\nu} (1 - 8f_\nu) \tilde{T}^2(k); & k > k_{nr}. \end{aligned} \quad (5)$$

In the following this approximation is merely used in justifying order of magnitude sensitivity of the SZ power spectrum to changing the fiducial neutrino mass; in our numerical calculations we employ a publically available code [30] to *precisely* determine $T(k, z)$. The effect of including nonlinear terms in f_ν on the matter power spectrum was investigated in several recent works, e.g. [31-33]. Indeed, this higher order effect modifies the matter power spectrum on scales of few Mpc and smaller, and in principle should be accounted for when data from future SZ surveys is available. In the current work this effect is ignored for simplicity. We can justify doing so by noting that the extra $O(f_\nu^2)$ term will only increase the sensitivity of σ_8 , and consequently also of the SZ effect, to the neutrino mass and thereby will increase the sensitivity of SZ-based cluster number counts and power spectrum to neutrino mass. In this regard the present analysis represents a conservative assessment of the capacity of cluster number counts and cluster correlations to constrain neutrino mass. Indeed, the latter studies [32,33] show that the factor $1 - 8f_\nu$ should be replaced by $\approx (1 - 9.8f_\nu)$ for $k \gg k_{nr}$. It is also clear that the f_ν^2 corrections to the matter power spectra are important when f_ν is sufficiently large. Indeed, neutrino masses twice or three times as large as the current 95% confidence upper limit on neutrino mass from WMAP (0.58 eV) were considered [31-33]. For the range of neutrino masses considered in this work, $M_\nu \leq 0.6$ eV, the nonlinear neutrino effects are smaller.

B. Cluster Mass Function

The basic quantity which describes the number density of clusters as a function of their mass and redshift - basic properties by which clusters are identified - is the mass function. As will be shown later, the total neutrino mass can be derived from comparison of the observed number of clusters at a given redshift-bin to the number predicted from the mass function, $\frac{dn(M; z)}{dM}$. The latter function is defined in terms of the differential cluster number in a redshift interval,

$$dN(M, z) = f_{sky} \frac{dn(M, z)}{dM} dV dM, \quad (6)$$

where dV is a volume element and f_{sky} is the observed sky fraction. The total number in a given interval Δz around z_i is

$$\Delta N(z_i) = f_{sky} \Delta z_i \frac{dV(z_i)}{dz} \int \frac{dn(M, z_i)}{dM} dM. \quad (7)$$

As noted earlier, the currently most optimal determination of the mass function is from extensive cosmological simulations. Here we adopt the mass function derived recently from a large set of collisionless cosmological simulations in Λ CDM cosmological model [34]. Expressing the mass function in the familiar form,

$$\frac{dn}{dM} = f(\sigma) \frac{\rho_m}{M} \frac{d \ln(\sigma^{-1})}{dM}, \quad (8)$$

these authors derived a fit of the form

$$f(\sigma) = A \left[\left(1 + \frac{\sigma}{b} \right)^{-a} \right] e^{-\frac{c}{\sigma^2}}, \quad (9)$$

where the parameters A , a , b and c were best-fit to the results of their simulations. The mass function does not have a universal form, a fact that becomes apparent by the deduced dependence of these fit parameters on both redshift and the overdensity at virialization, Δ_v .

III. SZ POWER SPECTRUM

The SZ effect is a unique probe of cosmological parameters and cluster properties; its statistical diagnostic value is reflected through number counts and the power spectrum of the CMB anisotropy it induces. The dependence of cluster number counts and cluster correlations on the total neutrino mass, and an assessment of the feasibility of actually determining it from their measurements, are our main objectives in this work. To this end, we carry out a precise calculation of the SZ signature imprinted by a cluster of mass M at redshift z . We then calculate the integrated statistical pattern of the SZ-induced CMB anisotropy projected on the sky, and the corresponding cluster number counts. Obviously, the ultimate practical issue is how well can clusters be detected by a specific CMB experiment (characterized by both detector noise and angular resolution) in the presence of the primary CMB anisotropy and the emission of foreground (point) sources.

The thermal component of the SZ effect induced by a cluster with optical depth $\tau \equiv \int n_e \sigma_T dl$ and gas temperature T_e induces a small level of fractional change in the CMB temperature [35,36]

$$\frac{\Delta T}{T} = y \mathcal{F}(x) \quad (10)$$

where $y \equiv \tau \Theta_e$ is the Comptonization parameter, $\Theta_e \equiv kT_e/(m_e c^2)$, and k , m_e , and c are the Boltzmann constant, electron mass and speed of light, respectively. n_e and σ_T are the gas number density and Thomson cross section, respectively, and the integration over the photon pathlength is along the line of sight. In the classical limit the spectral function reads

$$\mathcal{F}(x) = x \coth(x/2) - 4 \quad (11)$$

where $x \equiv h\nu/(kT)$ is the dimensionless CMB frequency, and h and T denote the Planck constant and CMB temperature, respectively. Note that in this work we ignore relativistic corrections [37, 38], whose weighted impact over the full temperature range of clusters is small. Since n_e is non-uniform and has a typical scale, the cluster core radius r_c

(as well as its temperature T_e which we here assume uniform $T_e(r) = T_0$ for simplicity), the projected 2D profile of the y -parameter on the sky, inherits this typical angular scale, that determines together with other parameters (as we discuss below) the SZ flux associated with the cluster and thereby the likelihood of its detection with a given CMB survey. The 2D Fourier transform of the projected 3D Comptonization parameter generated by an individual cluster is, e.g. [39]

$$\tilde{\xi}_\ell = \frac{4\pi r_c}{l_c^2} \int_0^\infty r^2 y(r) \frac{\sin(lr/l_c)}{(lr/l_c)} dr, \quad (12)$$

where $l_c \equiv d_A/r_c$ and the angular diameter distance in a flat Λ CDM model is

$$d_A(z) = \frac{c}{(1+z)H_0} \int_0^z \frac{dz'}{\sqrt{\Omega_m(1+z')^3 + \Omega_\Lambda}}, \quad (13)$$

with H_0 , Ω_m and Ω_Λ denoting the Hubble constant today and matter and vacuum energies in critical density units, respectively. Note that the neutrino energy density is contained in Ω_m since all neutrino masses considered in this work are certainly non-relativistic out to the highest-redshift clusters considered in this work, $z \approx 1$. The virial radius of the cluster is related to its virial mass via the relation $M_v = \frac{4\pi}{3} R_v^3 \Delta_v(z)$, where $\Delta_v(z)$ is the overdensity at virialization with respect to the background, calculated from the spherical collapse model in Λ CDM universe.

An expression for the virial radius, R_v , as a function of the virial mass, M_v , and the underlying cosmology can be derived noting that

$$M_v = \frac{4\pi}{3} R_v^3 \rho_v(z) = \frac{4\pi}{3} R_v^3 \Delta_v(z) \frac{\rho_c(z)}{\rho_c(0)} \rho_c(0), \quad (14)$$

where $\rho_c(z)$ and $\Delta_c(z) \equiv \rho_v(z)/\rho_c(z)$ denote the critical density and the virial overdensity at redshift z , respectively. This relation leads to

$$R_v = \left[\frac{3M_v}{4\pi\Delta_c(z)} \frac{\rho_c(0)}{\rho_c(z)} \frac{1}{\rho_c(0)} \right]^{1/3} = 1.69 \left[\frac{M}{M_{15}} \frac{18\pi^2}{\Delta_c(z)} \right]^{1/3} \left[\frac{\rho_c(0)}{\rho_c(z)} \right]^{1/3} \text{ Mpc}, \quad (15)$$

where M_{15} is the cluster mass in units of $10^{15} M_\odot$. Writing

$$\frac{\rho_c(0)}{\rho_c(z)} = \frac{H_0^2}{H(z)^2}, \quad (16)$$

and the explicit redshift dependence of the Hubble parameter

$$H^2(z) = H_0^2 [\Omega_\Lambda + \Omega_m(1+z)^3], \quad (17)$$

we obtain

$$\frac{\rho_c(0)}{\rho_c(z)} = \frac{1}{\Omega_\Lambda + \Omega_m(1+z)^3} = \frac{\Omega_m(1+z)^3}{\Omega_\Lambda + \Omega_m(1+z)^3} \frac{1}{\Omega_m(1+z)^3} \equiv \frac{\Omega_m(z)}{\Omega_m} \frac{1}{(1+z)^3}. \quad (18)$$

Substituting this relation in the expression for the virial radius leads to

$$R_v = 1.69 \left[\frac{M}{M_{15}} \frac{18\pi^2}{\Delta_c(z)} \right]^{1/3} \left[\frac{\Omega_m(z)}{\Omega_m} \right]^{1/3} \frac{1}{1+z} \text{ Mpc} \cdot h^{-1}. \quad (19)$$

Hot intracluster (IC) gas is assumed to follow a β density profile,

$$n_e(r) = n_{e,0} [1 + (r/r_c)^2]^{-3\beta/2} \quad (20)$$

with the observationally-deduced $\beta = 2/3$, and a core radius defined as $10r_c = R_v$. The central electron gas density is $n_{e,0} = \rho_{g,0}(X+1)/(2m_p)$, where X and m_p denote the Hydrogen mass fraction (taken to be 0.69) and the proton mass, whereas

$$\rho_{g,0} = \frac{f_g \cdot M_v}{4\pi r_c^3 \int_0^{10} x^2 (1+x^2)^{-3\beta/2} dx} \quad (21)$$

is the central gas density, assuming that IC gas constitutes a fraction $f_g = 0.12$ of the total virial mass. The virial expression is adopted for the gas temperature

$$k_B T_{e,0} = \frac{\mu m_p G}{3\beta} \frac{M_v}{R_v}, \quad (22)$$

valid for $R_v \gg r_c$, where $\mu = 0.59$ is the mean molecular weight. The resulting dependences of the core radius, gas density and temperature on the cluster mass and redshift obviously stem from these definitions.

A key quantity employed in the next section in the calculation of the signal-to-noise detection of an individual cluster of mass M at redshift z is the power spectrum generated by the cluster

$$C_l^{SZ}(M, z; M_\nu) = \frac{1}{4\pi} |\tilde{\xi}(l, M_\nu; M, z)|^2 \mathcal{F}^2(x). \quad (23)$$

Clearly, the total contribution from the entire cluster population to the SZ signal (which is irrelevant to this work) is obtained from Eq.(23) by a weighted integration over M and z with $\frac{dn}{dM} \frac{dV}{dz}$, i.e. integration over differential cluster number dN (Eq.6). The SZ power spectrum is shown in Fig.1 for the three fiducial neutrino masses considered in this work: 0.1 (black), 0.3 (blue), and 0.6 (red) eV. All power spectra were obtained by setting $\mathcal{F} = -2$ which corresponds to the Rayleigh-Jeans limit. The appreciable sensitivity to the assumed neutrino mass comes from both the strong dependence of the transfer function on f_ν (Eqs.2, 1 & 5), i.e. $\Delta\sigma_8/\sigma_8 \approx -8\Delta f_\nu$ and the scaling of the SZ power spectrum with high power of σ_8 , typically σ_8^7 .

The contribution to the SZ power spectrum from cluster correlations is typically an order of magnitude lower than the Poissonian component, and peaks on angular degree scales where it is overwhelmed by the primary CMB anisotropy. Consequently, its expected relative contribution to the angular power spectrum is small (e.g., [40, 41]) and we therefore do not consider it in our analysis. Also ignored is the small kinematic component of the SZ effect [36]. Had we included these two components in our analysis, cluster detection rate would have increased somewhat, improving our statistics and therefore lowering the uncertainty on neutrino masses, but these effects are very small.

IV. FISHER MATRIX ANALYSIS

Our cosmological model includes the normalization A and tilt n of the primordial scalar perturbations, neutrino, $\Omega_\nu h^2$, $\Omega_m h^2$, and baryon, $\Omega_b h^2$, energy densities, the Hubble parameter h in km/sec/Mpc units, dark energy equation of state w , optical depth for reionization τ , and the primordial helium abundance Y_p . The last two parameters do not directly affect the SZ quantities but are correlated with other cosmological parameters which might affect the uncertainty of these and indirectly impact neutrino mass when probed with SZ number counts (and power spectrum). We first carry out the forecasts for the primary CMB. This is done both with and without lensing extraction (LE). The corresponding Fisher matrices are denoted F^{pr} and F^{LE} , respectively.

The extremely steep dependence of the SZ effect on σ_8 is clearly expected to result in strong dependence of neutrino mass constraints on the fiducial neutrino mass. This follows from the fact that for lower neutrino masses (when A is fixed) σ_8 increases and as a result the SZ amplitude increases, boosting the signal-to-noise (\mathcal{S}/\mathcal{N}) of cluster detection and tightening the constraints on inferred neutrino mass. Clearly, the main cluster parameter which determines the magnitude of the SZ signal, and thereby whether or not it will be detected in a flux-limited survey, is the total mass. However, the cluster redshift is also of relevance, as explained above and will be further discussed below. Since the mean properties of the cluster population provide a good basis for estimating global parameters, their gaseous mass fraction could, in principle, be related directly to the ratio Ω_b/Ω_m (after accounting for the small contribution by the cluster member galaxies). However, in this work we adopt the fiducial value of the gas mass fraction deduced from the sample of SZ measurements with the BIMA & OVRO telescopes, $f_g = 0.12$ [42]. Due to the appreciable uncertainty in the measured value of f_g this cluster parameter is also treated as a model parameter in our Fisher matrix analysis.

In calculating the Fisher matrix for the primary CMB (with and without LE) we follow the standard approach which we do not reproduce here; details of the calculation can be found in (e.g.) [17].

A. M_ν from Cluster Number Counts and Correlations

As in, e.g., [43], we write for the Poissonian likelihood function for cluster number counts in the i 'th redshift bin

$$\mathcal{L}_i(N_i^p; N_i^o) \propto \frac{(N_i^p)^{N_i^o} \exp(-N_i^p)}{N_i^o!}, \quad (24)$$

where N_i^p is the predicted (for a given cosmological model and specified neutrino mass) and N_i^o the observed cluster number in the i 'th redshift bin. Note that here and in the following we use abbreviated notation and denote ΔN_i of Eq.(7) as N_i . If N_i^p is a function of several cosmological parameters λ_k , we may consider small deviations with respect to the expected fiducial value $N_i^o \approx N_i^p + \sum_k \frac{\partial N_i^p}{\partial \lambda_k} \Delta \lambda_k$. The Fisher matrix for cluster number counts can then be determined from the likelihood function

$$F_{jm}^N = -\frac{\partial^2 \ln \mathcal{L}}{\partial \lambda_j \partial \lambda_m} = \sum_i \frac{1}{N_i} \frac{\partial N_i}{\partial \lambda_j} \frac{\partial N_i}{\partial \lambda_m}. \quad (25)$$

The estimated uncertainty in the parameter λ_j is then

$$\Delta \lambda_j = (F_{jj}^N)^{-1/2}, \quad (26)$$

where we take the square root of the j 'th Fisher matrix element.

The second neutrino probe we employ in this work are measurements of the SZ power spectrum. Again, only those clusters which are detected at 5σ or better qualify for our 'simulated' sample. For the corresponding Fisher matrix we use the Fourier transform $P_c(k; z)$ of the cluster correlation function $C(r; z)$, as in [44]

$$F_{jm}^{P_c} = \sum_{a,i} \frac{\partial \ln(k_\perp^2 k_\parallel P_c)_{ai}}{\partial \lambda_j} \frac{\partial \ln(k_\perp^2 k_\parallel P_c)_{ai}}{\partial \lambda_m} \frac{(V_k V_{eff}(k))_{ai}}{2} \quad (27)$$

where the effective survey volume is

$$V_{eff}(k) = 4\pi f_{sky} \int r^2(z) \frac{dr}{dz} dz \left[\frac{n(z_i) P_c(k)}{1 + n(z_i) P_c(k)} \right]^2 \quad (28)$$

and $n(z_i)$ is the number density of detected clusters at the i 'th redshift bin. V_k is the k -space volume element

$$V_k = \frac{2\pi \Delta(k_\perp^2) \Delta k_\parallel}{(2\pi)^3}. \quad (29)$$

$P_c(k_\perp, k_\parallel; z)$, the cluster power spectrum, is

$$P_c(k_\perp, k_\parallel; z) = [1 + \beta(z) \mu^2] b^2(z) P(k; z) \quad (30)$$

where $k^2 = k_\perp^2 + k_\parallel^2$, $\mu \equiv k_\parallel/k$, $\beta(z) \equiv \frac{1}{b(z)} \frac{d(\ln D_{gr})}{d(\ln a)}$ and D_{gr} is the linear growth factor obtained from solving the equation governing the linear evolution of density perturbations δ

$$\frac{d^2 \delta}{da^2} + \left[\frac{2}{a} - \frac{1}{2a} \left(\frac{\Omega_m a^{-3} - 2\Omega_\Lambda}{\Omega_m a^{-3} + \Omega_\Lambda} \right) \right] \frac{\delta}{da} - \frac{3}{2} \frac{\Omega_m (1 - f_\nu)}{\Omega_m a^2 + \Omega_\Lambda a^5} \delta = 0 \quad (31)$$

where a is the scale factor, and $f_\nu \equiv \Omega_\nu/\Omega_m$ is the fraction of DM in the form of neutrinos. Here, the mass-averaged linear bias is

$$b(z) = \int dM \frac{dn(M, z)}{dM} \tilde{b}(M; z) / \int dM \frac{dn(M, z)}{dM} \quad (32)$$

where $\tilde{b}(M; z)$ is obtained from hydrodynamical simulations [45].

The total Fisher matrix that includes cluster number counts combined with either the primordial or lensed CMB is $F_{jm}^{pr} + F_{jm}^N$ or $F_{jm}^{LE} + F_{jm}^N$, respectively, and the uncertainty in the parameter λ_j is similar to that in Eq.(26), except for the fact that now F_{jm}^N is replaced with either $F_{jm}^{pr} + F_{jm}^N$ or $F_{jm}^{LE} + F_{jm}^N$. Similarly, from the power spectrum we obtain $F_{jm}^{pr} + F_{jm}^c$ or $F_{jm}^{LE} + F_{jm}^c$, respectively.

Integrated cluster quantities, such as number counts and the power spectrum, obviously depend on the assumed mass range. Our nominal mass range is taken to be $10^{13} - 3 \times 10^{15} M_\odot$. While it is doubtful whether our description of IC gas properties is valid at the low mass end of this range, we have verified that our results are insensitive to the exact value of the low mass end by repeating the calculations with three different values for the low mass cutoff, with only a negligible fraction (2% and 0.2% for EPIC and SPT, respectively) of the clusters in our mass range have masses smaller than $5 \times 10^{13} h^{-1} M_\odot$. This is an important consistency check since the assumption of virialization (Eqs. 14-22) is expected to break down at around this value, and since the cluster mass cannot be deduced in a

model-independent way, it is reassuring that the detection threshold is set such that clusters for which our model breaks down are not included in the sample. This essentially is the case as long as the detection threshold is taken to be at the 5σ significance level. The upper mass limit of this range is in accord with recent detailed joint data analyses (e.g. [46]) that have resulted in reliable mass estimates that are already very close to the above value. Here too, raising the upper mass to $10^{16} M_\odot$ has little impact on the uncertainty in inferred M_ν .

To estimate the \mathcal{S}/\mathcal{N} with which a cluster can be detected in a survey, we assume that the main noise sources are the instrument, primary CMB anisotropy, and point source emission. We ignore other astrophysical foregrounds, such as free-free emission, synchrotron radiation and dust, due to their Galactic origin and the planned removal of this sky region in the PLANCK and EPIC data analysis. Galactic contamination in the SPT and ACT survey is minimized by selecting a radio-quiet sky region. Optimal (minimum variance) *unbiased* filters can be constructed for cluster detection with the resulting \mathcal{S}/\mathcal{N} variance [47, 48] characterized by minimum confusion noise

$$\left(\frac{\mathcal{S}}{\mathcal{N}}\right)^2 = \sum_i \int \frac{ldl}{2\pi} \frac{|\tilde{\xi}_l|^2(\nu_i)}{[C_l^{det}(\nu_i) + C_l^{CMB} + C_l^{PS}(\nu_i)]}, \quad (33)$$

which is merely proportional to the ratio of the power spectra of signal and noise weighted by Fourier space volume ($\propto l$) and summed over all accessible multipoles. Contribution to the \mathcal{S}/\mathcal{N} from scales below the beamsize are exponentially damped

$$C_l^{det} = (\Delta_T \theta_b)^2 e^{l^2 \sigma_b^2} \quad (34)$$

where $\theta_b = \sqrt{8 \ln(2)} \sigma_b$. Δ_T is a noise-equivalent-temperature (NET) of the experiment, and the sum over i runs over all the detector frequency channels. The relevant parameters for the PLANCK instrument, SPT, and EPIC are listed in Table I. The adopted power spectrum of point sources is [49]

$$C_l^{PS} = A_{ps} (x_Q/x)^{-4} (e^x - 1)^4 x^{-4} e^{-2x}, \quad (35)$$

where $A_{ps} = 0.015 \mu K^2 \text{-str}$, $x_Q \equiv (h\nu_Q)/(kT)$, and $\nu_Q = 40.7 \text{ GHz}$ is WMAP's Q-band. C_l^{PS} , Δ_T , and θ_b are all frequency-dependent.

As shown in Eqs.(12) & (23) the SZ power spectrum is a function of the cluster core radius, θ_c , which in itself is a function of M and z (Eqs. 19 & 20). Therefore, one can define the \mathcal{S}/\mathcal{N} per a single cluster in the M - z cell

$$\left(\frac{\mathcal{S}}{\mathcal{N}}\right)_{M,z}^2 \equiv \sum_i \int \frac{ldl}{2\pi} \frac{|\tilde{\xi}_l(M, z; \nu_i)|^2}{[C_l^{det}(\nu_i) + C_l^{CMB} + C_l^{PS}(\nu_i)]}, \quad (36)$$

where $\tilde{\xi}_l(M, z; \nu_i)$ is given by Eq.(12); recall though that the cluster core radius is a function of both mass and redshift. This measure, together with the mass function, which determines the number density in each of the M - z cells, can be used to estimate how many clusters will be detected at a given cell by a specific experiment. This criterion is employed in the next section.

V. RESULTS

In this work we have adopted the Λ CDM cosmological model with WMAP best-fit parameters. The cluster population is described in terms of the mass function of Tinker et al. [34, 45], and the (hot) IC gas mass fraction was taken at the level deduced from SZ observations, $f_g \simeq 0.12$. IC gas has been assumed to be isothermal with a beta density profile. It is important to note that in this analysis no priors were set neither on the cosmological parameters nor on f_g . We reiterate that changing neutrino masses over the range $[0.1, 0.6] \text{ eV}$ changes σ_8 by $\sim 25\%$. Since the SZ effect strongly depends on σ_8 , we expect observational measures of the effect to show a corresponding level of sensitivity to varying M_ν , as is indeed evident from Figure 1.

Our analysis includes several inherent noise sources - detector noise, and the noise due to the primary CMB anisotropy and extragalactic point sources. We first calculate the distribution of $(\mathcal{S}/\mathcal{N})_{M,z}$ with which clusters of mass M at redshift z will be detected (Eq. 36) in the PLANCK, SPT and proposed EPIC surveys. As is clear from Eq.(36) the clusters detectability likelihood depends on both their masses and redshifts; the mass and redshift together determine the \mathcal{S}/\mathcal{N} , as is clear from the fact that the gas temperature and core radius (both physical and certainly its angular projection on the sky) depend on both M and z (Eqs. 19 & 20). We set the level of statistical detectability to 5σ .

Our basic results for neutrino mass uncertainty based on cluster number counts and power spectrum from SZ surveys with the ongoing PLANCK, SPT, and proposed EPIC projects are presented in Tables II and III for the

fiducial neutrino masses, 0.1, 0.3, and 0.6 eV. In Table II we show (from left to right) the expected uncertainty on the inferred M_ν from the primordial CMB (both temperature anisotropy and polarization), primary CMB and cluster SZ number counts, primary CMB and cluster correlation, and finally the constraints from joint primary CMB, cluster number counts and power spectrum. Table III is the same as Table II, but the priors are from LE. It is particularly interesting to see that if M_ν is $\sim 0.1\text{eV}$, then the joint primordial CMB, cluster abundance and correlation analysis for PLANCK yields $\sigma_{M_\nu} = 0.28\text{eV}$, whereas the constraint from CMB LE is 0.14eV .

Similar results for ACT are shown in Table V. This project is viewed here as a generic ground-based SZ survey experiment with deep exposure on a very small patch of the sky. Our goal is to optimize the scanning strategy for neutrino mass inference. The analysis presented here clearly illustrates that the uncertainty on neutrino masses can be reduced by $\sim 1/2$ when the survey area increases from 200deg^2 to $4,000\text{deg}^2$. Indeed, increasing f_{sky} results in a higher noise per sky-pixel, which lowers the detection significance of many clusters, but with the 5σ detection-threshold we adopt here it turns out that only the smallest clusters are removed from our sample and this is outweighed by improving the statistics of massive/nearby clusters by virtue of increasing f_{sky} . Specifically, we considered four fiducial ACT modes; ACT-A, B, C and D (Table IV). ACT-A refers to the nominal ACT experiment that covers 200deg^2 of the sky. ACT-B, C and D scan 400, 1000 and 4,000 deg^2 , respectively. The larger f_{sky} , the shorter is the integration time available per sky-pixel, and assuming the integration is uniform over the sky and that the instrumental noise is inversely proportional to the integration time, $\Delta_T \propto t_{int}^{-1/2}$, we can rescale ACT-A to the other three modes. While ACT-A has very low noise it is limited by the lower statistics because of the survey area, 0.5% of the sky. Results listed in Tables V and VI clearly illustrate that eventually the gain in sky area (in the cases of ACT-C and D) result in a notable improvement in neutrino mass constraints. The lesson from this is that observing a larger sky-patch is preferable, at least for neutrino mass inference and for a CMB telescope with ACT-like specifications. It should be noted here that the priors, i.e. constraints that come from either primordial CMB or LE that we adopted in these tables come from PLANCK, not ACT itself (which should also be affected by changing f_{sky}), and are for a fixed $f_{sky} = 0.65$.

An important aspect of the theoretical treatment is careful selection of the mass range. In principle, we could compare expected and observed number counts on the entire 2D M - z space, if it was realistic to reliably deduce cluster masses (from the ‘blind’ surveys considered here). Since cluster mass inference is highly model-dependent we always integrate the cluster distribution over mass and consider number counts in redshift-space only, as described earlier (Eqs. 25 & 27). Integrating the *expected* number counts and cluster correlation over mass we have to impose a low mass cutoff, thereby removing all low-mass clusters from our sample. As noted already, this is motivated mainly by the fact that objects that have detectable mass of sufficiently hot ($\geq 1\text{ keV}$) gas, and for which our theoretical description is still valid - including aspects such as the gas density profile, mass-temperature scaling, and indeed the attainment of hydrostatic equilibrium in the first place - do not include very poor clusters and groups of galaxies. We have checked and verified that our results are robust with respect to changing this low mass cutoff to the lowest cluster mass of $10^{13}M_\odot$ we consider in this work. This obviously reflects the consistency between our theoretically selected value of the low mass cutoff and the high significance that we require for the threshold for SZ detection.

Formation of clusters is relatively late in the ΛCDM model, with the vast majority of medium to high mass clusters forming at $z < 1$ (as is clear from plots of the probability distributions of formation times in [46]). We checked that essentially irrespective of the fiducial neutrino mass considered, the contribution to the Fisher matrix saturates at $z_{max} \lesssim 1$. Higher-redshift clusters are simply not sufficiently massive and in addition project on too small angular scales to be detected.

Redshift binning may also introduce some bias; by increasing bin width the diagnostic capability is weakened, but the impact of random fluctuations e.g. modelling errors that bias the redshift of cluster formation is reduced. This motivated us to determine an optimal redshift-binning in our number counts analysis by binning the redshift interval $[0 - 1]$ into 10, 20 and 40 linearly spaced redshift shells. We found that increasing this number from 10 to 20 improves the statistical error on the deduced neutrino mass by not more than $\sim 30\%$. Further binning refinement to 40 shells reduces the error by at most 15%, implying that further increase in the number of shells does not reduce the statistical uncertainty but may come at a cost of a higher level of systematic error. All results reported in this work using cluster number counts were obtained by binning the simulated data into 40 redshift bins. For the cluster correlation probe we used only 10 redshift shells; as in [51] we choose k-binning in Eq.(27) to be wide enough for different bins to be uncorrelated. We assume $\Delta z = 0.1$ for this analysis and $\Delta k = 0.005 h\text{Mpc}^{-1}$ in the k-range $[0.005-0.1] h\text{Mpc}^{-1}$.

The most important source of uncertainty in modeling cluster abundance and internal properties is the mass function. Current uncertainties in this basic function were explicitly included in our analysis. Continued extensive cosmological hydrodynamical simulations (e.g. [52]) are likely to result in a significantly more precise description of this function across the cluster mass range. In contrast, uncertainties stemming from using simple models for the spatial profiles of the gas density and temperature are of secondary importance, simply because these are much reduced when calculating integrated SZ measures and, more generally, will have little effect on cluster detection. After all, the magnitude of the effect in a cluster is not determined by each of these quantities separately (in the non-relativistic

limit that is valid for our purpose here), but rather by the integrated gas pressure along the line of sight. Thus, even though central regions of clusters are roughly isothermal, and the gas density profile is well approximated by the beta profile, realistic deviations from isothermal beta profile for the pressure, when integrated across a cluster and over the mass function, introduce a level of uncertainty that is ignorable for our purposes here. Mass function normalization and three additional shape parameters (Eq. 9) are included in our analysis.

VI. DISCUSSION

The CMB is perhaps one of best understood and model-independent underpinnings of modern cosmology. Temperature anisotropy and polarization measurements of the primary CMB signal already taught us a great deal about the geometry of the universe, its energy content, reionization history, etc. With the imminent detection of the lensing-induced signal of the CMB by PLANCK, and possibly even the inflationary-induced B-mode polarization (if inflation is indeed related to GUT scale physics), the CMB may open new windows into the physics of neutrinos as well as processes that occurred in the GUT era; the latter are well beyond the reach of any present or future terrestrial experiment.

However, the capacity of primary CMB alone to constrain $\sim Mpc$ cosmology is rather limited; even CMB lensing by the LSS, a sensitive probe of neutrino masses, takes place on considerably larger physical scales. In addition, standard forecasts of LE performance widely build on the assumption that the CMB signal is gaussian in the absence of lensing, and any nongaussianity present in the data can be attributed to lensing of the CMB. It should be emphasized that the results for neutrino masses derived from CMB and LE reported here, and elsewhere in the literature, always make this simplifying assumption. However, non-gaussianity can also be induced by astrophysical sources. The issue of primordial nongaussianity is still open and should be considered as another source of confusion. On the relevant angular scales secondary CMB signals, such as the SZ effect, are known to be present. These are typically nongaussian and can interfere with LE.

Structure on Mpc scales probes the entire evolution history of matter perturbations down to these scales. This is especially relevant to neutrino physics via the effect of neutrino free streaming on these and larger scales. Indeed, Lya observations can supplement the CMB on these scales but since the astrophysics of the former is more involved it is desirable to consider other probes of clustering on Mpc scales to complement Lya , as well as other traditional probes such as galaxy clustering, shear measurements, etc., or at the very least to serve as a consistency check. The possibility of using cluster catalogues in constraining neutrino masses has already been discussed in [19]. More generally, extraction of cosmological parameters, such as Ω_b , Ω_Λ , from cluster number counts - in conjugation with other cosmological probes - is widely discussed in the literature, e.g. [43,53].

In this work we considered the prospect of SZ surveys to constrain neutrino masses. We have shown that using cluster number abundance alone neutrino mass uncertainties may be constrained to the $\sim 0.36 - 0.55$ eV levels by PLANCK and $\sim 2 - 3$ times weaker by SPT SZ surveys alone, on a wide range of allowed neutrino masses ($M_\nu < 0.6$ eV). The proposed EPIC satellite with its SZ survey of thousands of clusters will be able to set impressive constraints on neutrino masses at the level that will enable us to constrain models of inverted mass hierarchy (where $M_\nu > 0.1$ eV). For this seemingly promising potential to be realized a full account of systematics has to be achieved; we elaborate on mass-function uncertainties below. Systematics, such as unknown gas fraction f_g , are easily accounted for by simply including them as free parameters in our analysis; with predicted hundreds (SPT) or thousands (PLANCK and EPIC) clusters we have sufficient freedom to include other parameters, such as f_g , in addition to M_ν and A . It is quite likely that follow-up X-ray observations will yield a more precisely determined value of f_g , a possibility we clearly do not consider in this work as we assumed no prior on f_g .

Another subtlety comes from possible degeneracy with Ω_{de} . Including degeneracy with dark energy in our framework is indeed possible with the code employed here for the transfer function [30] as it was developed especially for the purpose of calculating the impact of large scale structure suppression by both neutrino free streaming and accelerated expansion of the universe induced by dark energy. A very crude estimate of this effect can be obtained by fixing the CDM component, Ω_{dm} , and changing Ω_ν on the expense of Ω_{de} , but since the total energy density is assumed to be fixed to its critical value, and since both neutrino (with a total mass in the range considered here) and dark energy do not clump on galaxy cluster scales, we can conclude that - at least to first approximation - allowing all three Ω_ν , Ω_{de} and Ω_{dm} to vary (subject to the constraint that the total energy density is fixed) does not substantially affect our results.

The impact of sub-eV neutrino masses will obviously be reflected also in the superposed SZ power from the population of clusters. We have calculated the full power spectrum by integrating the expression for a single cluster (specified in Section III) over the mass function for three neutrino masses, 0.1, 0.3, and 0.6 eV. Results of this calculation are shown in Fig. 1 by the black, blue, and red curves, respectively. Since σ_8 is approximately proportional to $1 - 8f_\nu$, changing neutrino mass in the range $[0.1 - 0.6]$ eV corresponds to varying f_ν in the range $[0.7 - 4.3] \times 10^{-2}$; this

introduces a fractional change $\Delta\sigma_8/\sigma_8 \approx -8\Delta f_\nu$. The steep dependence of SZ power on σ_8 translates to a relative change of $\approx 56f_\nu$. From Fig. 1 we see that this factor amounts to an overall variation of the peak power by a factor of ~ 3 for the above range of neutrino masses. Note though that in our calculations we used the precise transfer function and did not employ this crude approximation which we mention here only for the sake of obtaining a rough estimate of the SZ sensitivity to changing neutrino masses. Confusion with the CMB primary and other confusing signals renders this neutrino signature less diagnostically useful as compared with the more optimized cluster SZ number counts or correlations. It is important to note that the steep SZ power spectrum dependence on neutrino masses does not *directly* imply similar sensitivity in number counts. The only direct effect of the power spectrum dependence on M_ν is that large neutrino mass decreases the SZ power spectrum, and therefore the S/N with which galaxy clusters are detected, thereby boosting the uncertainty on neutrino masses as is illustrated in Table II.

Another tantalizing possibility is using these large cluster surveys to *simultaneously* calibrate the mass function and determine neutrino mass. This will help reducing possible bias that could be caused by miss-calibration of the mass function. In our analysis we adopted the functional form of the Tinker mass function, Eqs.(8) & (9), and considered the shape parameters as free parameters in the statistical analysis, adopting the central values reported in [34]. To test the robustness of our results to changing the mass function used in the parameter estimation we repeated the analysis with a different mass function which was similarly derived from hydrodynamical simulation - the Jenkins mass function [54]. We found that the constraints on neutrino mass do not change by more than 4%, and in most cases the differences do not exceed the 1-2% level.

It is clear that more can be done to refine the analysis presented here since, admittedly, cluster physics and statistical properties of the cluster population are model-dependent. However, we believe that the adoption of a rigorous criterion for cluster detection in M - z space, assuming implementation of well-known unbiased optimal filters (in conjugation with the need to reject low mass clusters from our sample), the realization that the statistics improve when neutrino masses are lower as σ_8 increases, the use of a high precision transfer function for neutrinos in our theoretical SZ model, and optimal binning in redshift space, all these factors together constitute important steps towards achieving a high precision probe of neutrino masses. These features lend credibility to the results presented in this work. The results are encouraging: Cluster number counts, and to a lesser extent cluster correlations, may indeed be reliable neutrino probes if carefully analyzed. The utility of this probe largely depends on the neutrino mass; the lower the mass, the tighter is the constraint (as is shown in Table II and explained above). The prospects will only be further enhanced when SZ surveys will be jointly analyzed with results from extensive X-ray surveys.

-
- [1] MacTavish, C. J., et al. 2006, ApJ, 647, 799.
 - [2] Komatsu, E., et al. 2010, arXiv:1001.4538
 - [3] Cooray, A. R. 1999, AAP, 348, 31.
 - [4] Abazajian, K., & Dodelson, S. 2003, PRL, 91, 041301.
 - [5] Hannestad, S., Tu, H., & Wong, Y. Y. 2006, JCAP, 6, 25.
 - [6] Kitching, T. D., Heavens, A. F., Verde, L., Serra, P., & Melchiorri, A. 2008, PRD, 77, 103008.
 - [7] Hu, W., Eisenstein, D. J., & Tegmark, M. 1998, PRL, 80, 5255.
 - [8] Tegmark, M., et al. 2004, PRD, 69, 103501.
 - [9] Hannestad, S. 2003, JCAP, 5, 4.
 - [10] Tegmark, M., et al. 2006, PRD, 74, 123507.
 - [11] Thomas, S. A., Abdalla, F. B., & Lahav, O. 2010, PRL, 105, 031301
 - [12] Croft, R. A. C., Hu, W., & Davé, R. 1999, PRL, 83, 1092.
 - [13] Goobar, A., Hannestad, S., Mörtzell, E., & Tu, H. 2006, JCAP, 6, 19
 - [14] Seljak, U., Slosar, A., & McDonald, P. 2006, JCAP, 10, 14.
 - [15] Gratton, S., Lewis, A., & Efstathiou, G. 2008, PRD, 77, 083507.
 - [16] Kaplinghat, M., Knox, L., & Song, Y.-S. 2003, PRL, 91, 241301.
 - [17] Lesgourgues, J., Perotto, L., Pastor, S., & Piat, M. 2006, PRD, 73, 045021.
 - [18] Perotto, L., Lesgourgues, J., Hannestad, S., Tu, H., & Y Y Wong, Y. 2006, JCAP, 10, 13
 - [19] Wang, S., Haiman, Z., Hu, W., Khoury, J., & May, M. 2005, PRL, 95, 011302
 - [20] Bock, J., et al., arXiv:0906.1188
 - [21] Smith, K.M., et al., arXiv:0811.3916
 - [22] Fukuda, Y., et al. 1998, PRL, 81, 1562
 - [23] Cleveland, B. T., et al. 1998, ApJ, 496, 505
 - [24] Fukuda, Y., et al. 1996, PRL, 77, 1683
 - [25] Rephaeli Y., 1995, An. Rev. Astron. Astro, 33, 541-579.
 - [26] Birkinshaw, M., 1999, Pyes. Rep, 310, 97-195.
 - [27] Carlstrom, J. E., Holder, G. P., & Reese, E. D., 2002, An. Rev. Astron. Astro, 40, 643-680.
 - [28] Bardeen, J. M., Bond, J. R., Kaiser, N., & Szalay, A. S. 1986, ApJ, 304, 15

- [29] Lesgourgues, J., & Pastor, S. 2006, Phys. Rep., 429, 307
- [30] Kiakotou, Elgaroy & Lahav, astro-ph/0709.0253
- [31] Saito, S., Takada, M., & Taruya, A. 2008, PRL, 100, 191301
- [32] Brandbyge, J., Hannestad, S., Haugbølle, T., & Thomsen, B. 2008, JCAP, 8, 20
- [33] Wong, Y. Y. Y. 2008, JCAP, 10, 35
- [34] Tinker, J. et al. 2008, ApJ, 688, 709
- [35] Sunyaev R.A., Zeldovich Y.B., 1972, Comments. Astrophys. Space Phys., 4, 173-178.
- [36] Sunyaev R.A., Zel'dovich Y.B., 1980, MNRAS, 190, 413-420.
- [37] Rephaeli, Y. 1995, ApJ, 445, 33
- [38] Shimon, M., & Rephaeli, Y. 2004, New Astronomy, 9, 69
- [39] Komatsu, E., & Seljak, U. 2002, MNRAS, 336, 1256
- [40] Komatsu, E., & Kitayama, T. 1999, ApJL 526, L1
- [41] Cooray, A., Baumann, D., & Sigurdson, K. 2005, Background Microwave Radiation and Intracluster Cosmology, 309
- [42] LaRoque, S. J., Bonamente, M., Carlstrom, J. E., Joy, M. K., Nagai, D., Reese, E. D., & Dawson, K. S. 2006, ApJ, 652, 917
- [43] Holder, G., Haiman, Z., & Mohr, J. J. 2001, ApJL, 560, L111
- [44] Wang, S., Khoury, J., Haiman, Z., & May, M. 2004, PRD, 70, 123008
- [45] Tinker, J. L., Robertson, B. E., Kravtsov, A. V., Klypin, A., Warren, M. S., Yepes, G., & Gottlober, S. 2010, arXiv:1001.3162
- [46] Lemze, D., Broadhurst, T., Rephaeli, Y., Barkana, R., & Umetsu, K. 2009, ApJL, 701, 1336
- [47] Haehnelt, M. G., & Tegmark, M. 1996, MNRAS, 279, 545
- [48] Geisbüsch, J., & Hobson, M. P. 2007, MNRAS, 382, 158
- [49] Bennett, C. L., et al. 2003, ApJS, 148, 97
- [50] Hu, W., & Haiman, Z. 2003, PRD, 68, 063004
- [51] Cunha, C. E., & Evrard, A. E. 2010, PRD, 81, 083509
- [52] Cunha, C., Huterer, D., & Frieman, J. A. 2009, PRD, 80, 063532
- [53] Jenkins, A., et al. 2001, MNRAS, 321, 372

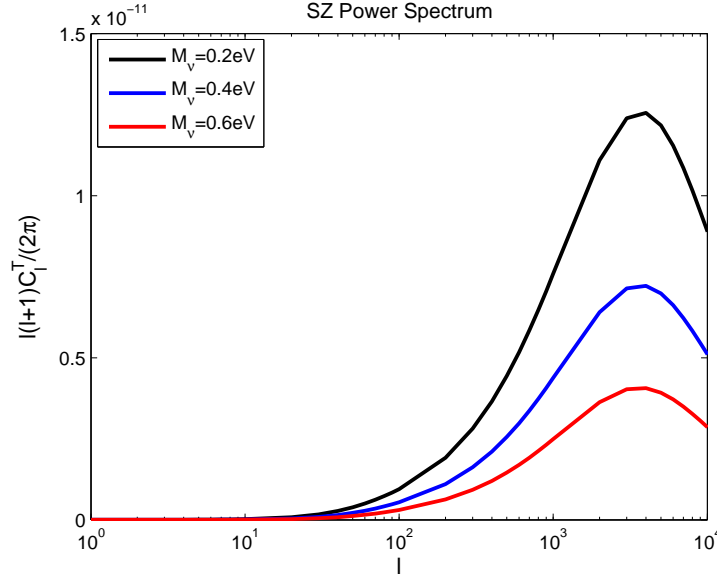


FIG. 1: SZ power spectrum for three neutrino masses: 0.1 (black), 0.3 (blue) and 0.6 eV (red). As explained in the text, the dependence $\sigma_8 \propto 1 - 8f_\nu$ translates to a relative change of $\approx 56f_\nu$ in the value of σ_8 when the total neutrino mass assumes values in the range 0.1 – 0.6 eV.

Experiment	f_{sky}	$\nu[\text{GHz}]$	$\theta_b[1']$	$\Delta_T[\mu\text{K}]$
PLANCK	0.65	30	33	4.4
		44	23	6.5
		70	14	9.8
		100	9.5	6.8
		143	7.1	6.0
		217	5.0	13.1
		353	5.0	40.1
		545	5.0	401
		856	5.0	18300
SPT	0.10	150	1.0	13.4
		274	0.52	71.4
		345	0.29	583.9
EPIC (4K)	0.65	30	28	0.50
		45	19	0.30
		70	12	0.21
		100	8.4	0.22
		150	5.6	0.25
		220	3.8	0.66
		340	2.5	2.24
		500	1.7	9.41
		850	1.0	740.0

TABLE I: Sensitivity parameters for Planck, SPT, and EPIC: f_{sky} is the observed fraction of the sky, ν_0 is the central channel frequency (in GHz), θ_b is the FWHM (Full-Width at Half-Maximum) in arcminutes, and Δ_T is the temperature sensitivity per pixel in μK . Polarization sensitivity is $\Delta_E = \Delta_B = \sqrt{2}\Delta_T$, except for the 545 and 857 GHz bands of PLANCK which are unpolarized. We assume all the frequency bands can be used for primordial CMB and LE, but for the purpose of cluster detection we assumed that only the 100, 143 & 353 GHz (PLANCK) and 100, 150 & 340 GHz channels (EPIC) can be reliably used, since these are the least foreground-contaminated bands.

Experiment	$M_\nu[\text{eV}]$	$\sigma_{M_\nu}[\text{eV}](\text{prim.})$	$\sigma_{M_\nu}[\text{eV}](\text{prim.}+\text{N}(z))$	$\sigma_{M_\nu}[\text{eV}](\text{prim.}+\text{Pc}(z))$	$\sigma_{M_\nu}[\text{eV}](\text{prim.}+\text{N}(z)+\text{Pc}(z))$
SPT	0.1	2.02	0.46	1.21	0.44
	0.3		1.25	1.37	1.01
	0.6		1.52	1.55	1.27
PLANCK	0.1	0.67	0.36	0.55	0.28
	0.3		0.55	0.60	0.42
	0.6		0.55	0.63	0.50
EPIC	0.1	0.34	0.13	0.23	0.12
	0.3		0.25	0.26	0.20
	0.6		0.30	0.30	0.25

TABLE II: Statistical uncertainty on total neutrino mass from cluster number counts obtained from PLANCK, SPT, and EPIC SZ surveys (no LE). Shown are neutrino mass uncertainties (1σ) expected to be obtained from the respective planned surveys. We consider σ_{M_ν} assuming fiducial masses 0.1, 0.3 and 0.6 eV. We show the results from CMB alone, CMB+cluster number counts $\text{N}(z)$, CMB+cluster correlation Pc , and CMB+ $\text{N}(z)$ + Pc .

Experiment	$M_\nu [eV]$	$\sigma_{M_\nu} [eV] (LE)$	$\sigma_{M_\nu} [eV] [LE+N(z)]$	$\sigma_{M_\nu} [eV] [LE+Pc(z)]$	$\sigma_{M_\nu} [eV] [LE+N(z)+Pc(z)]$
SPT	0.1	0.52	0.35	0.41	0.25
	0.3		0.50	0.44	0.34
	0.6		0.51	0.49	0.43
PLANCK	0.1	0.14	0.12	0.12	0.11
	0.3		0.12	0.13	0.12
	0.6		0.13	0.14	0.13
EPIC	0.1	0.05	0.04	0.04	0.04
	0.3		0.04	0.04	0.04
	0.6		0.04	0.04	0.04

TABLE III: Same as in Table II but with LE priors.

Experiment	deg^2	$\nu [GHz]$	$\theta_b [1']$	$\Delta_T [\mu K]$
ACT-A	200	145	1.7	2.0
		280	0.93	8.8
ACT-B	400	145	1.7	2.83
		280	0.93	12.45
ACT-C	1,000	145	1.7	4.47
		280	0.93	19.68
ACT-D	4,000	145	1.7	8.94
		280	0.93	39.35

TABLE IV: ACT-A, B, C and D: ACT-A is rescaled to B, C and D by assuming $f_{sky} \propto t_{int}^{-1}$ and $\Delta_T \propto t_{int}^{-1/2}$.

Experiment	$\sigma_{M_\nu} [eV] (\text{prim.})$	$\sigma_{M_\nu} [eV] [\text{prim.}+N(z)]$	$\sigma_{M_\nu} [eV] [\text{prim.}+Pc(z)]$	$\sigma_{M_\nu} [eV] [\text{prim.}+N(z)+Pc(z)]$
ACT-A	0.67	0.61	0.66	0.61
ACT-B	0.67	0.60	0.65	0.59
ACT-C	0.67	0.51	0.64	0.49
ACT-D	0.67	0.40	0.61	0.36

TABLE V: Statistical uncertainty on total neutrino mass from cluster number counts and cluster correlation (similar to Table II) obtained from ACT-A, B, C and D SZ surveys (no LE). Shown are neutrino mass uncertainties (1σ) expected to be obtained from the respective planned surveys. We consider σ_{M_ν} assuming fiducial mass 0.1 eV. We show the results from CMB alone, CMB+cluster number counts $N(z)$, CMB+cluster correlation Pc , and CMB+ $N(z)+Pc$. Primordial CMB priors from PLANCK are considered.

Experiment	$\sigma_{M_\nu} [eV] (LE)$	$\sigma_{M_\nu} [eV] [LE+N(z)]$	$\sigma_{M_\nu} [eV] [LE+Pc(z)]$	$\sigma_{M_\nu} [eV] [LE+N(z)+Pc(z)]$
ACT-A	0.14	0.14	0.14	0.14
ACT-B	0.14	0.14	0.14	0.14
ACT-C	0.14	0.14	0.14	0.13
ACT-D	0.14	0.13	0.13	0.12

TABLE VI: Same as in Table V but with LE priors.